CARDIFF UNIVERSITY
PRIFYSGOL CAERDYDD

ORCA – Online Research @ Cardiff

This is an Open Access document downloaded from ORCA, Cardiff University's institutional repository:https://orca.cardiff.ac.uk/id/eprint/108726/

This is the author's version of a work that was submitted to / accepted for publication.

Citation for final published version:

Dimitriadis, Stavros , Salis, Christos and Linden, David 2018. A novel, fast and efficient single-sensor automatic sleep-stage classification based on complementary cross-frequency coupling estimates. Clinical Neurophysiology 129 (4) , pp. 815-828. 10.1016/j.clinph.2017.12.039

Publishers page: http://dx.doi.org/10.1016/j.clinph.2017.12.039

Please note:
Changes made as a result of publishing processes such as copy-editing, formatting and page numbers may not be reflected in this version. For the definitive version of this publication, please refer to the published source. You are advised to consult the publisher's version if you wish to cite this paper.

This version is being made available in accordance with publisher policies. See http://orca.cf.ac.uk/policies.html for usage policies. Copyright and moral rights for publications made available in ORCA are retained by the copyright holders.

Highlights

- Cross-Frequency Coupling (CFC) is a key mechanism of brain interactions in sleep.
- Different estimates of CFC contribute to high sleep stage classification accuracy.
- Single-Sensor Automatic Single Sensor Classification can provide a means of alternative low-cost sleep monitoring.

A Novel, Fast and Efficient Single-Sensor Automatic Sleep-Stage Classification Based on Complementary Cross-Frequency Coupling Estimates

Stavros I. Dimitriadis[1-4*], Christos Salis[5], David Linden[1,2,3,6]

[1]Institute of Psychological Medicine and Clinical Neurosciences, Cardiff University School of Medicine, Cardiff, UK
[2] School of Psychology, Cardiff University School of Medicine, Cardiff, UK
[3]Cardiff University Brain Research Imaging Center (CUBRIC), School of Psychology, Cardiff University, Cardiff, UK
[4]Neuroinformatics Group, (CUBRIC), School of Psychology, Cardiff University, Cardiff, UK
[5]University of Western Macedonia, Department of Informatics and Telecommunications Engineering, Kozani, Greece
[6]Neuroscience and Mental Health Research Institute (NMHRI) Psychology, Cardiff, UK

Abstract:

Objective: Limitations of the manual scoring of polysomnograms, which include data from electroencephalogram (EEG), electro-oculogram (EOG), electrocardiogram (ECG) and electromyogram (EMG) channels, have long been recognized. Manual staging is resource intensive and time consuming, and considerable effort must be spent to ensure inter-rater reliability. There is thus great interest in techniques based on signal processing and machine learning for a completely Automatic Sleep Stage Classification (ASSC).

Methods: In this paper, we present a single-EEG-sensor ASSC technique based on the dynamic reconfiguration of different aspects of cross-frequency coupling (CFC) estimated between predefined frequency pairs over 5 s epoch lengths. The proposed analytic scheme is demonstrated using the PhysioNet Sleep European Data Format (EDF) Database with repeat recordings from 20 healthy young adults.

Results: We achieved very high classification sensitivity, specificity and accuracy of **96.2 ± 2.2%, 94.2 ± 2.3%,** and **94.4 ± 2.2% across 20 folds**, respectively, and a high mean F1 score (92%, range 90–94%) when a multi-class Naive Bayes classifier was applied.

Conclusions: Our method outperformed the accuracy of previous studies not only on different datasets but also on the same database.

Significance: Single-sensor ASSC makes the entire methodology appropriate for longitudinal monitoring using wearable EEG in real-world and laboratory-oriented environments.

Keywords: EEG; sleep stages; EEG sub-bands; machine learning algorithms; phase-to-amplitude coupling

***Corresponding author**:
Dr. Dimitriadis Stavros
MARIE-CURIE COFUND EU-UK Research Fellow
School of Medicine,
Cardiff University, UK
CUBRIC Neuroimaging Centre, Cardiff, UK
Email: stidimitriadis@gmail.com; DimitriadisS@cardiff.ac.uk

1. Introduction

Sleep as a basic human function is characterized by continuous alterations in brain, muscle, eye, heart and respiratory activity. These multi-dimensional alterations are monitored with appropriate equipment in a sleep laboratory and are measured during a full night of sleep. Typically, these polysomnographic recordings include the electroencephalogram (EEG), electro-oculogram (EOG), electromyogram (EMG) and electrocardiogram (ECG). Physiologically, sleep stages can be split into two types: rapid eye movement (REM sleep) and non-rapid eye movement (non-REM sleep) (Steriade and McCarley, 1990). The latter consists of 4 stages (called N1, N2, N3 and N4). The process of assigning a sleep stage to every epoch of polysomnographic recordings is called sleep scoring. Sleep staging is a very important step in sleep research and for the clinical interpretation of the polysomnogram (for a review, see Aboalayon et al., 2016).

In clinical daily routine, sleep studies are performed for the diagnosis of pathologies such as circadian rhythm disorders, epilepsy, sleep apnea, insomnia and hypersomnia (Panossian and Wikman , 2009). Sleep scoring is often based on a visual inspection of the polysomnographic recordings to establish a hypnogram that dynamically represents the different sleep stages. Sleep experts usually follow well-established rules for manual sleep scoring based on state-of-the-art guidelines (Hobson, 1969). Rechtschaffen and Kales (1968) introduced rules for the labelling of each segment of 30 s as Awake, S1–S4 or REM sleep stage. A more recent sleep manual proposed by the American Academy of Sleep Medicine (AASM) in 2007 (Iber et al., 2005) combines the non-REM stages S3 and S4 into a single stage of deep sleep (called N3), also known as slow-wave sleep (SWS). Both manuals suggest the use of EEG channels, two in the R&K (Hobson, 1969) manual and three in the AASM manual (Iber et al., 2005): 2 EOG electrodes and one EMG electrode.

Sleep stage scoring is the gold standard for the analysis of human sleep (Agarwal and Gotman, 2005). While many sleep laboratories use the traditional manual sleep stage scoring of neurophysiological recordings to produce the hypnogram, recent years have witnessed a burst of proposed methods for automatic or semi-automatic sleep staging (e.g., Agarwal and Gotman, 2005; Becq et al., 2005; Berthomier et al., 2007; Ma et al., 2011; Itil et al., 1969; Koley and Dey, 2012; Krakovská and Mezeiová, 2011; Larsen and Walter, 1970; Schaltenbrand et al., 1996; Sheng-Fu et al., 2012; Pan et al., 2012; Stanus et al., 1987; Gudmundsson et al., 2005; Šušmáková and Krakovská, 2008; Huang et al., 2002). The different methods for ASSC generally extract features from the signals to analyse each temporal segment

(epoch) and use classification algorithms to detect/predict the sleep stages (Güneş et al., 2010; Zoubek et al., 2007; Sousa et al., 2015). These features focus on a time-domain analysis (Tsai et al., 2009; Gudmundsson et al., 2005; *Khalighi et al., 2011*), frequency-domain analysis (Zhovna and Shallom, 2008; Yu et al., 2012) and time-frequency-domain analysis (Ebrahimi et al., 2008; Li et al., 2009).

Complementarily, complexity and nonlinear measures have been successfully used (Kuo and Liang, 2011; Phan et al., 2013; Fell et al., 1996). In some ASSC systems, an appropriate pre-processing step of manipulating the selected features is added prior to the classification step. This pre-processing step includes feature selection and/or dimensionality reduction (Koley and Dey, 2012; Zoubek et al., 2007; Sen et al., 2014). The main scope of this step is to reduce the dimension of the estimated features. A wide range of machine learning-based classification methods, such as Linear Discriminant Analysis (LDA) (Sousa et al., 2015; Weiss et al., 2011), Artificial Neural Networks (ANN) (Liu et al., 2010; Dursun et al., 2012), Support Vector Machine (SVM) (Huang et al., 2013; Brignol et al., 2012; Yu et al., 2012; Lainef et al., 2015), K-Nearest Neighbour (KNN) (Kuo and Liang, 2011; Liu et al., 2010), Decision Trees (DT) (Schaltenbrand et al., 1996; Pan et al., 2012) and SVM-DT (Lan et al., 2015) have been adopted for sleep stage classification.

The clinical uptake of ASSC systems has been hindered by low accuracy, sensitivity and specificity. The classification accuracies varied among the ASSC methods reported in the literature, ranging from 70% to 94%, while the sensitivity and specificity remained lower than 90%. Some studies on ASSC systems have considered using a single EEG channel, but many issues remained unsolved, such as the high similarity of the EEG characteristics between REM and S1 (Lan et al., 2015; Krakovská and Mezeiová, 2011; Estrada et al., 2004), which has lowered the overall classification performance.

Cortical excitability following rhythmic changes produces neuronal oscillations with different cell population sizes and therefore different spatial scales (Fries, 2005). It is well known that low-frequency rhythms are established as a dominant coupling mode in distant neuronal interactions and long temporal windows. In the opposite, high-frequency rhythms are established as a dominant coupling mode in local neuronal interactions and short temporal windows (von Stein and Sarnthein, 2000). The continuous interactions between anatomical substrates/backbone and the cortical oscillatory patterns give the brain the flexibility to simultaneously work at multiple spatio-temporal scales (Buzsaki and Draguhn, 2004 ; Buzsaki and Watson,2012).

The distinct neuronal oscillations that travel with a dominant frequency rhythm are not independent, and the lower frequencies in particular can modulate the oscillations of higher-frequency brain rhythms (Jensen and Colgin, 2007). The interactions between brain rhythms with different frequency profiles are called cross-frequency coupling (CFC), which can be categorized as phase synchronization, amplitude co-modulation (correlation of the envelope: Bruns and Eckhorn, 2004) and phase-amplitude coupling (PAC; Pittman-Polletta et al., 2014; Dimitriadis et al., 2015, 2016a, b).

PAC is believed to be the substrate of neural coding and information exchange between the micro and macro scales of the neural ensembles of the brain (von Stein and Sarnthein, 2000; Jensen and Colgin, 2007; Axmacher et al., 2010; Canolty and Knight, 2010). It seems that low-frequency oscillations regulate the information exchange between brain areas by modulating the excitability levels of local neural ensembles (von Stein and Sarnthein, 2000; Fries, 2005), while their phase also affects high-frequency activity at the level of individual neurons and their spiking rates (Canolty and Knight, 2010). PAC facilitates interactions between neuronal ensembles with similar phase and quantifies the strength of interactions between high-frequency bands with the phase of lower-frequency bands within low-frequency-dependent temporal windows (Allen et al., 2011). To quantify the PAC between brain signals of different frequency profiles, we used three basic algorithms: a) one based on iPLV (Dimitriadis et al., 2015, 2016), b) one based on the mean vector length (MVL) (Canolty et al., 2006) and c) the Modulation Index (MI) (Tort et al., 2008).

Another type of CFC interaction between brain areas that oscillate on a different frequency rhythm is the correlation of the envelope of two brain signals that encapsulates brain activity of different spectral profiles (Bruns and Eckhorn, 2004). It was found that inter-frequency coupling, specifically the correlation of the amplitude envelopes between low- and high-frequency components, was established between non-phase-coupled patches in awake monkeys between areas located within their visual cortex (Bruns et al., 2001). It seems that envelope-to-signal correlation is a complementary type of CFC to PAC and reflects the transmission of temporally modulated brain activity from a source area to a target area in many conditions. Since the mechanism of neuronal exchange of information underlying the nature of this CFC metric is basic and the type of coupling is non-linear, this CFC type is of general interest for exploring basic communication mechanisms in many situations.

The formation of new memories demands the coordination of neural activity across widespread brain regions. In both humans and animals, the hippocampus is believed to support the formation of new associative or contextually mediated memories (Clemens et al., 2009).

During the consolidation of new memories at the system level, mnemonic representations of items, thoughts, new faces, and the like initially rely on the hippocampus and are subsequently thought to travel to neocortical sites for more permanent storage. Sleep has this privileged role for facilitating this information transfer (Born and Wilhelm, 2012). Mechanistically, consolidation processes have been demonstrated to rely on systematic interactions between the three basic neuronal oscillations that characterize non–rapid eye movement (NREM) sleep: slow oscillations, spindles and ripples (Staresina et al., 2015). The hierarchical role of these three components was revealed via phase-to-amplitude coupling based on a mean vector length estimator. A recent study untangled hippocampo-cortical CFC as the basic mechanism that mediates memory consolidation during sleep (Maingret et al., 2016). The authors provided a clear link between sharp-wave ripples, δ waves and ripples. Logothetis et al. (2012) demonstrated CFC coupling between hippocampo-cortical areas during a subcortical silence and off-line memory consolidation. Amiri et al. (2016) demonstrated an enhanced PAC in deep sleep and in the onset zone of focal epilepsy.

Based on the aforementioned knowledge regarding CFC brain interactions, the multiplexity of brain interactions across different daily and laboratory-oriented tasks and our knowledge regarding sleep functionality in both humans and primates, we aimed in the present study to explore the effectiveness of different CFC estimates for automatic sleep stage classification in normal human populations.

In this paper, we propose a fast and efficient single-sensor ASSC that achieves multi-class classification by combining estimations of cross-frequency coupling with a multi-class Naïve Bayesian classifier. First, we estimated the relative power on predefined frequencies extracted via a wavelet analysis. Subsequently, complementary cross-frequency coupling (CFC) estimators were adopted based on the following: a) phase-to-amplitude coupling (PAC) to quantify how the phase of the lower frequency brain rhythms modulates the amplitude of the higher oscillations, b) the correlation of the envelopes, c) the modulation index and d) a proposed complex version of the modulation index. The entire approach was followed in a temporal segment (epoch) of 5 sec and within the two EEG bipolar sensors (FPz-Cz & Pz-Oz) and between every possible pair of the studied frequency bands. In previous applications, PAC has shown promise as a biomarker for amnestic mild cognitive impairment (Dimitriadis et al., 2015a), dyslexia (Dimitriadis et al., 2016), or mild traumatic brain injury (Antonakakis et al., 2016). We extracted the most important features using the infinite feature selection and fed them into a multi-class Naïve Bayesian classifier following a 20-fold cross-validation scheme. The entire approach was also validated in a second dataset.

In brief, the proposed ASSC methodology, which is described in more detail below, consists of four main steps: (i) estimation of CFC estimates per cross-frequency pair in temporal segments 5 s in length in both EEG channels) and the relative power within each frequency, (ii) feature selection using sequential selection and cross-validation within the training dataset and (iii) classification using a multi-class Naïve Bayesian classifier based on the features selected in (ii). External validation of the proposed methodology in a second dataset was performed using the features selected from the first one (iv).

The layout of the paper is as follows. In Section 2, we describe the subject population, the experiments that were performed, and the methods used for data pre-processing steps of the proposed pipeline and the classification procedure. The results are presented in Section 3, and Section 4 is devoted to the discussion.

2. Materials and Methods

The proposed sleep stage classification approach can be divided in four steps. Fig. 1 demonstrates those four steps, which can be summarized as follows:

1) Signal processing and extraction of wavelet components within the predefined frequencies
2) Estimation of the features based on relative power and different CFC estimators per frequency pair
3) Feature selection
4) Classification of the sleep stages

[**Figure 1** around here]

2.1. Polysomnographic database

The **polysomnographic** dataset that we used to present and evaluate the proposed novel methodology is a publicly available sleep PSG dataset (Kemp et al., 2000) demonstrated as part of the PhysioNet repository (Goldberger et al., 2000), which can be downloaded (from The Sleep-EDF Database [Expanded]", Physionet.org). The brain activity was recorded from two electrode pairs, the Fpz-Cz and Pz-Oz, instead of the standard C3-A2 and C4-A1. The sleep stages were assigned to the following stages/conditions: wake (W), REM (R), non-R stages 1–4 (N1, N2, N3, N4), movement and not scored. The sleep scoring of each epoch of 30 s length

was realized by six experts following the Rechtschaffen and Kales guidelines (Hobson, 1969). For our study, we removed from further analysis the very small number of movement and not scored epochs (not scored epochs were mostly at the beginning or end of each recording). We also retained N3 and N4 as distinct sleep stages. In the entire dataset, we detected 61 epochs with movements, while only 17 had artefacts due to movements. Across the cohort, the maximum number of movement epochs was 12.

The adopted open-access dataset consisted of 20 healthy subjects (10 male / 10 female), aged 25–34 years. There were two 20-h recordings per subject. EEG recordings were sampled at 100 Hz, and the epoch duration was 30 s.

2.2 **Feature Extraction**

Both EEG channel recordings were decomposed every 5 s with the Maximal Overlap Discrete Wavelet Transform (MODWT) wavelet method and Daubechies wavelet filters (dau4).

The wavelet signals were then mapped to one of eight predefined frequency ranges. The reason why we preferred a wavelet decomposition over predefined bandpass filtering of the sleep EEG recordings is to obtain a more accurate temporal resolution of the well-established frequency ranges and to distinguish true from artefactual sleep activity. For that reason, we combined EOG and EMG recordings with wavelet time series to remove signals directly linked to eye movements and muscle activity. The predefined frequencies were as follows: low-δ {0.1-1.5 Hz}, high-δ (K-Complex) {1.6-4 Hz}, θ {4-8 Hz}, α_1 {8-10 Hz}, α_2 {10-13 Hz}, β_1 (spindle) {14-20 Hz}, β_2 {21-30 Hz} and γ_1 {31 – 45 Hz}.

We split the δ frequency band to capture slow-wave activity and to focus on the well-known frequency profile of K-complex that suppresses cortical arousal in response to any external stimulus and plays a key role in sleep-based memory consolidation (Cash et al., 2009). Additionally, β brain rhythms were further split into low and high to capture sleep spindle activity via CFC. Sleep spindles occur during stage 2 sleep and often follow the occurrence of K-Complex. Sleep spindles result from thalamo-cortical interactions and have been found to a) suppress the presence of disruptive external sounds (a correlation has been revealed between the brain activity in the thalamus and the subject's ability to be calm) (Dang-Vu et al., 2010) and b) be associated with the integration of new information into existing knowledge (Tamminen et al., 2010) as well as directed remembering and forgetting (Saletin et al., 2011; fast sleep spindles).

We estimated five types of features: 1) the relative signal power for each frequency band in the time domain based on the Maximal overlap discrete wavelet transform (MODWT), 2) the phase-to-amplitude coupling (PAC) estimated between every possible pair of frequencies, 3) the correlation coefficient between the envelopes of the frequency bands as an amplitude-amplitude cross-frequency coupling (AAC) estimator, 4) a novel complexed version of the modulation index (CMI) for estimating the phase-to-amplitude coupling between every possible pair of frequencies and 5) the original modulation index (MI). All the cross-frequency coupling estimators were computed between all possible pairs of the eight predefined frequency bands (8*7/2=28 combinations).

All features were estimated within each epoch of 30 s length and by adopting a sliding non-overlapped window of 5 s duration, which resulted in 6 temporal non-overlapped segments per 30 s. The entire analysis led to the extraction of 120 (8 relative signal power + 28 Phase-to-Amplitude coupling (PAC) + 28 Amplitude-to-Amplitude coupling (AAC) + 28 Phase-to-Amplitude coupling (CMI) + 28 Phase-to-Amplitude coupling (MI)) total features per epoch. All the features were mapped in the [0,1] interval independently for each EEG channel.

2.2.1 Relative Signal Power

EEG recordings of every 5 s sub-epoch were decomposed using the Maximal overlap discrete wavelet transform (MODWT) wavelet method and Daubechies wavelet filters (dau4). The outcome of this process was a time series with frequency profile that corresponded to the predefined frequency bands.

We estimated the relative power of each bandpass frequency signal segment in the time domain with the following equations:

$$SP(fr) = \sum_{fr=1}^{frequencies} \sum_{t=1}^{T} filtered(fr,t)\text{^}2 \quad (1)$$

$$RSP(fr) = \frac{SP(fr)}{\sum_{fr=1}^{frequencies} SP(fr)} \quad (2)$$

The first equation quantifies the signal power (SP) of each frequency as the sum of the filtered signal squared per sample (1), while equation (2) divides the SP by the sum of the SP from all the frequencies, which provides the relative signal power (RSP). The entire approach was repeated for every epoch, sub-epoch, EEG sensor pair and subject.

2.2.2 Cross-Frequency Coupling Estimations

2.2.2.1 Phase-to-Amplitude Coupling Cross-Frequency Coupling (PAC)

CFC quantifies the strength of interactions between time series of different frequency contents. It can be estimated both within and between sensors (Canolty and Knight, 2010; Buzsáki, 2010; Buzsáki et al., 2013). CFC can be estimated between power – power, amplitude – amplitude and amplitude-phase representations of two time series with different frequency contents. These representations can be derived by filtering twice one time series (within) or filtering once two time series (between). The most common type of CFC interaction is phase-to-amplitude coupling (PAC), and it is the most common in the literature (Voytec et al., 2010). The PAC algorithm for a single EEG sensor is described below.

Let $x(i_{sensor}, t)$ be the EEG time series at the i_{sensor}-th recording site, and t=1, 2,.... T be the sample points. Given a bandpassed filtered signal $x(i_{sensor}, t)$, CFC is quantified under the notion that the phase of the lower-frequency (LF) oscillations modulates the amplitude of the higher-frequency (HF) oscillations. The following equations describe the complex representations of both (LF) $z_{LF}(t)$ and (HF) oscillations $z_{HF}(t)$ produced via the Hilbert transform (HT[.]).

$$z_{LF}(t) = HT[x_{LF}(t)] = |z_{LF}(t)| e^{i\phi_{LF}(t)} = A_{LF}(t) e^{i\phi_{LF}(t)},\ z_{HF}(t) = HT[x_{HF}(t)] = |z_{HF}(t)| e^{i\phi_{HF}(t)} = A_{HF}(t)\ e^{i\phi_{HF}(t)}$$

The next step in the PAC algorithm is the estimation of the envelope of the HF oscillation $A_{HF}(t)$, which is then decomposed via the wavelet. We selected the component within the frequency range of LF oscillations. Subsequently, the resulting time series is again Hilbert transformed to obtain its phase time series that describes its phase dynamics φ'(t):

$$z'(t) = \mathrm{HT}[\ A_{\mathrm{HF,LF}}(t)\ ] = |z'(t)|\, e^{i\phi'_{\mathrm{HF}}(t)} = |z'(t)|\, e^{i\phi_{\mathrm{LF}\to\mathrm{HF}}(t)}$$

The aforementioned complex equation analytically describes the modulation of the amplitude of HF oscillation by the phase of LF oscillation.

The phase consistency between those two time series can be measured not only by the original phase locking value (PLV) estimator (Lachaux et al., 1999) but also from its imaginary portion of PLV. The imaginary part of PLV (iPLV) can be used as a synchronization index that quantifies the strength of CFC-PAC coupling.

PLV is defined as follows:

$$PLV = \frac{1}{T} * \sum_{t=1}^{T} e^{i(\phi_{LF}(t) - \phi_{HF}(t))} \quad (3)$$

iPLV is defined as follows:

$$Im\,PLV = \frac{1}{T} * \left| Im \sum_{t=1}^{T} e^{i(\phi_{LF}(t) - \phi_{HF}(t))} \right| \quad (4)$$

The iPLV is an estimator that is less affected than PLV by the volume conduction effect. Using iPLV for quantifying the strength of CFC interactions is an advantage over volume conduction. iPLV is more sensitive to non-zero phase lag, and for that reason, it is more resistant to any self-interactions that are directly linked to volume conductions (Nolte et al., 2004). For further details and applications, interested readers can see our previous work (Dimitriadis et al., 2016; Antonakakis et al., 2016).

In the present study, as was previously mentioned, we used the wavelet signals that corresponded to the eight frequency bands, which means that PAC was estimated for 8*7/2=28 cross-frequency pairs, e.g., δ^{φ} - θ^{A} and δ^{φ} - α_1^{A}, where φ and A denote the phase and amplitude, respectively, of each frequency band. Figure 2 demonstrates the pre-processing steps of the PAC estimator using a 30 s epoch from the wake stage of subject 1.

[**Figure 2** around here]

2.2.2.2 Amplitude-to-Amplitude Cross-Frequency Coupling (AAC)

The complex analytic representation of each signal, as derived via the MODWT approach $z_F(t)$, was then Hilbert transformed (HT[.]).

$$z_F(t) = HT[x_F(t)] = |z_F(t)| e^{i\phi_F(t)} = A_F(t) e^{i\phi_F(t)}$$

Next, the envelope of the frequency oscillations $A_F(t)$ was squared to express the power of the signal in the time domain. Subsequently, the correlation coefficient between every pair of the derived time series was estimated to express the associations between specific frequency pairs.

$$AAC = corrcoef(A_{F_1}(t).\hat{}2, A_{F_2}(t).\hat{}2) \quad (5)$$

In the present study, as was previously mentioned, we used the wavelet signals that corresponded to the eight frequency bands, which means that AAC was estimated for 8*7/2=28 cross-frequency pairs, e.g., δ^A - θ^A and δ^A - $\alpha_1{}^A$, where A denotes the amplitude of the envelope of each frequency band. In Fig.3, we demonstrated the pre-processing steps of the AAC estimator for the detection of coupling between θ and β_1 rhythms using a 30 s epoch from the wake stage of subject 1. The original signal **(A)** was bandpass filtered into both **(B)** a high-frequency β_1 (13–20 Hz) component, where its envelope was extracted, and **(C)** a low-frequency θ (4–8 Hz) component, where its envelope was also extracted. In **(D),** the envelopes of the bandpassed θ (4–8 Hz) and β_1 (13–20 Hz) were presented into a common plot. **(E)** Finally, we estimated the point-wise squared time series of the envelopes to obtain the power time series. The AAC was estimated on these power time series using correlation coefficient via the equation 5.

[**Figure 3** around here]

2.2.2.3 A Complex Version of the Modulation Index (CMI)

The Modulation Index (MI) has been presented as a novel estimator for constructing a phase-amplitude plot (comodulogram) that demonstrates the strength of how the phase of a low frequency modulates the amplitude of the high frequency within a raw signal (Tort et al., 2010).

Let $x_{raw}(t)$ denote the raw signal of one of the EEG recordings. The MI is calculated for every pair of frequencies, creating a phase-amplitude plot. The steps for estimating the modulation index are as follows:

1) First, $x_{raw}(t)$ is filtered at the two frequency ranges, the low-frequency f_p and the high-frequency f_A. We denote the filtered signals as $x_{fp}(t)$ and $x_{fA}(t)$.

2) The time series of the phases of $x_{fp}(t)$ [denoted as $\phi_{fp}(t)$] is obtained from the standard Hilbert transform of $x_{fp}(t)$.

The Hilbert transform is also applied to $x_{fA}(t)$ to extract the time series of the amplitude envelope of $x_{fA}(t)$ [denoted as $A_{fA}(t)$].

A composite time series is constructed [$\phi_{fp}(t)$, $A_{fA}(t)$], giving the amplitude of the f_A oscillation at each phase of the f_p rhythm.

3) Next, the phases $\phi_{fp}(t)$ are binned (here we used 20 bins of the 360° of range 18°), and the mean of A_{fA} over each phase bin is calculated. We denote by (j) the mean A_{fA} value at the phase bin j.

4) At the last step, we normalize the mean amplitude by dividing each bin value by the sum over the bins:

$$P(j) = \frac{< A_{f_A} >_{\phi_{f_p}}(j)}{\sum_{k=1}^{N} < A_{f_A} >_{\phi_{f_p}}(k)} \quad (6)$$

where N denotes the number of phase bins (here, N=20 s).

Here, instead of equation 6, we use the following transformation based on the composite signal:

$$z_F(t) = HT[x_F(t)] = |z_F(t)| e^{i\phi_F(t)} = A_F(t) e^{i\phi_F(t)}$$

which is defined by the following equation:

$$CMI = \frac{\left| \sum_{k=1}^{N} < (A_{f\,A}(k)) > exp^{i<(\phi_{f\,p}(k))>} \right|}{N} \quad (7)$$

where we obtain the product of the mean A_{fA} within each phase bin with the mean ϕ_{fp} within each phase bin N.

In the present study, we employed the wavelet signals that corresponded to the eight frequency bands, which means that CMI was estimated for each one of 8*7/2=28 cross-frequency pairs, e.g., δ^A - θ^A and δ^A - $\alpha_1{}^A$, where A denotes the amplitude of the envelope of each frequency band. Figure 4 demonstrates the pre-processing steps of the CMI estimator using a 30 s epoch from the wake stage of subject 1. We used the first-epoch EEG signal from the Fpz-Cz sensor of subject 1 during the wake condition **(A)**. θ and β_1 frequency pair was adopted to estimate the coupling using CMI and to be comparable with PAC and AAC. To estimate θ-β_1 with CMI estimator, the raw signal was bandpass filtered into **(B)** a low-frequency θ (4–8 Hz) component, where its phase was extracted. In **(C)**, the amplitude of the high-frequency β_1 (13–20 Hz) component was presented while in **(D)** the mean amplitude of the high-frequency component was estimated within each **(E)** phase bin extracted from the phase of the low-frequency component. Finally, the CMI was estimated based on the average complex values of mean amplitude and mean phase within each bin via the equation 7. Here, we used 20 phase bins.

[**Figure 4** around here]

2.2.2.4 The Modulation Index (MI)

The original defined MI (Tort et al., 2010) was estimated via equation 6. Figure 4 demonstrates the pre-processing steps of the MI estimator using a 30 s epoch from the wake stage of subject 1. Equation 4 is calculated based on the amplitude and phase bins presented in Fig. 4D, E.

Here, we used the wavelet signals that corresponded to the eight frequency bands, which means that MI was estimated for 8*7/2=28 cross-frequency pairs, e.g., δ^A - θ^A and δ^A - $\alpha_1{}^A$, where A denotes the amplitude of the envelope of each frequency band.

2.2.2.5 A graphical Visualization of Cross-Frequency Interactions

For every epoch of 5 sec and for the four cross-frequency coupling estimators, we quantified the cross-frequency interactions. There were 28 possible pair-wise combinations of the eight brain rhythms, in which γ_1 frequency cannot be a modulator but only a modulated frequency. We visualized these 28 cross-frequency interactions using a graphical representation in which the nodes denote seven out of eight brain rhythms, the direction of arrows illustrates the direction of the modulation, and the colour encodes the strength of the coupling. In our example, we adopted epoch 1 from N1 of the first subject from the training dataset using the phase-to-amplitude estimator. It is important to underline that, in the present study, we used a single sensor for the estimation of the four cross-frequency interactions and relative power estimates. For every epoch of 5 sec and for each of the four CFC estimates, we quantified the pair-wise cross-frequency interactions among the eight brain rhythms. Fig. 5.E provides a complementary visualization scheme for the cross-frequency coupling interactions, called a comodulogram, in a graphical layout compared to a tabular representation (Dimitriadis et al., 2015a, 2016a).

2.3 Feature Selection

We ranked the entire set of estimated features using the infinite feature selection method introduced in Deng et al. (2010). We applied the feature selection strategy to the training set in every fold of the leave-one-out cross-validation scheme (LOOCV; see next section). Finally,

we selected the features that were consistently selected in the top 40% across the 20 folds. For every fold, we obtained a ranking of the 120 features, and we finally selected the number of features that consistently appeared on the top 40% across the 20 folds (see also Fig. 1).

2.4 Machine learning and classification

We accessed the generalizability of the entire approach using 20-fold cross-validation. Specifically, in each fold, we used the features extracted from a single subject for testing and all other recordings for training. The methodology was tested with both available EEG electrodes (Fpz-Cz and Pz-Oz). Each subject's recordings were used only once for testing, thus obtaining a one-to-one correspondence of cross-validation folds and test subjects.

We report the scoring performance using the best electrode, which was Fpz-Cz. Group-averaged confusion matrices are reported to present the average classification performance per sleep stage, while the mean accuracy, sensitivity, specificity and F1 score are also reported.

We used five different classifiers: a) the k-nearest neighbour, b) the Naïve Bayesian multi-class classifier (Linear and Kernel), c) the extreme-learning machine (ELM) (Linear, RBF) (Huang et al., 2012), d) linear discriminant analysis (LDA) and e) the multi-class support vector machines (multi-SVM – libsvm toolbox) (Linear, RBF) (Chang and Lin, 2011).

To avoid the effect of imbalanced sleep stage representation and to present true performance measures (accuracy, sensitivity, specificity, and F1 score) and confusion matrices, we randomly sampled the sleep stages across each fold to obtain an equal representation of each sleep stage across sleep stages and subjects. We repeated the 20-fold cross-validation 100 times.

2.5 Second Polysomnographic Database

The adopted second open-access dataset consisted of 77 healthy subjects (36 males aged 59.01 ± 23.31 / 41 females aged 58.53 ± 21.6) with an age range of 26–101 years. There were whole-night polysomnographic sleep recordings containing EEG (from Fpz-Cz and Pz-Oz electrode locations), EOG (horizontal), submental chin EMG, one from each subject. EEG recordings were sampled at 100 Hz, and the epoch duration was 30 s.

2.6 Computational time of the proposed ASSC

Automatic sleep scoring by a neurologist requires 3-4 hours for a single hypnogram (Lainscsek et al., 2013). Our algorithm can estimate the selected features and produce the ASSC of a single subject based on the training set in 8.9 ± 1.3 min on average (depending on the duration of the sleep recordings) using a multi-core processor and parallelizing the MATLAB code in a MATLAB environment. We estimated the computational time on the second dataset, which was 9.2 ± 1.5.

3. Results

3.1 Discriminative Features of Sleep Stages

In the following tables, we demonstrate selected features from the pool of four complementary cross-frequency estimators (Table 1.A) adopted here and the relative power estimates (Table 1.B). In Table 1.A, we denoted with a 'number' the selected features derived from each of the four CFC estimators, which were 36 out of 120. Using a criterion of consistency of features on the top 40% (0.4*120=48 features) across the 20 folds, we finally selected 36 features from the first training set. The same set of features was used for external validation of the entire approach to the second dataset.

Fig. 5 (A-D) illustrates the comodulograms of the four CFC estimators adopted in the present study averaged across epochs at each sleep stage from a single subject. At every subplot, a comodulogram (2D matrix) illustrates for every pair of stages (sleep stages +wake) and CFC estimators, the cross-frequency interactions between every possible pair of frequencies. The x-axis are the frequencies of the modulator, while on the y-axis are the frequencies of the modulated brain rhythm. In Fig.5 (A-D), rows refer to the comodulograms of each of the four CFC estimators and the columns to the sleeps stages and the wake state. This figure provides a common framework for someone to understand the complementary information of cross-frequency interactions that has been estimated by PAC,AAC,CMI and MI. Clearly, one can detect the differentiation of the strength of the coupling across sleep stages for PAC (Fig. 5A), AAC (Fig. 5B) and CMI (Fig. 5C) compared to MI (Fig. 5D), which mostly detected modulations between low, high-δ and θ brain rhythms. PAC coupling was elevated between low, high-δ and the rest of the frequency subcomponents in deep sleep compared to NREM and W. A graphical layout of the CFC interactions is illustrated in Fig.5E where nodes refer to brain rhythms, the color of the arrow indicates the strength of the coupling while the direction of the arrows are directed to the modulated frequencies. For example, in Fig.5E,the

red arrow indicates the modulation of δ frequency to the α_2 At each epoch of 5 sec and for each of the four cross-frequency coupling estimates, all possible pair-wise frequency interactions were estimated, as shown in the graphical representation. In Fig.5E ,PAC couplings are demonstrated estimated for the first epoch of the N1 sleep stage of subject 1 in the first dataset.

Fig. 6 illustrates the RP of each frequency subcomponent at each sleep stage and the wake period from a single subject (same as in Fig. 6) after averaging across all epochs from a single scan. It is obvious that low-δ {0.1-1.5 Hz}, high-δ (K-Complex) {1.6-4 Hz} and θ {4-8 Hz} demonstrated significant differences at the sleep stages and the wake period. We denoted with '*' the significant differences of RP across the frequencies at every sleep stage and wake condition. (* Wilcoxon Rank Sum Test, $p < 0.01$, Bonferroni corrected $p' < p/28$ where 28 denotes the possible pairs of the 8 frequencies)

Table 1.A Selected features from the four CFC estimators

γ_1	1		1	3	3		2	
β_2		3	1		2,3	2		
β_1	1,3	1	1,3		1,3			
α_2			3	1,2				
α_1	1	1	2,3					
θ	1,2,4	1,2,4						
high-δ	1,2,4							
low-δ								
	low-δ	high-δ	θ	α_1	α_2	β_1	β_2	γ_1

where 1,2,3,4 refer to PAC,AAC,CMI & MI correspondingly

Table 1.B Selected features from RP.

	low-δ	high-δ	θ	α_1	α_2	β_1	β_2	γ_1
RP	✓	✓	✓					

[Figures 5,6 around here]

3.2 Sleep State Classification Performance

We achieved very high classification accuracy, sensitivity and specificity of **96.2 ± 2.2%, 94.2 ± 2.3%,** and **94.4 ± 2.2%, respectively, across the 20 folds**. Complementarily, the mean F1 score was also high (92%, range 90–94%). The aforementioned results were followed by the application of the multi-class Naive Bayes classifier (with kernel). All of our measures were first averaged across folds at each repetition, and then we estimated the means and standard deviation across 100 repetitions of the 20 folds.

The best results were achieved with the Fpz-Cz sensor. **Table 2** demonstrates the averaged confusion matrix across the 20 folds. Diagonal elements refer to the % of match between experts and our algorithm, while off-diagonal elements illustrate the % of mismatch. The most correctly classified sleep stage was N4, followed by N3, W, N2, R and N1. Most misclassifications of N1 occurred in the R and W stages, for N2 in N3 and R, for N3 in R and W, for N4 in N3, for R in NI and N3 and for W in N4 and R.

Table 2. Averaged Confusion Matrix Across the 20 Folds based on the best-performing Fpz-Cz channel (%).

	N1 (Algorithm)	**N2 (Algorithm)**	**N3 (Algorithm)**	**N4 (Algorithm)**	**R (Algorithm)**	**W (Algorithm)**
N1 (Expert)	**94.1 (4.9)**				0.6 (0.03)	
N2 (Expert)		**94.7 (4.1)**				
N3 (Expert)	0.03 (0.02)	2.8 (0.03)	**98.8 (3.8)**	0.09 (0.03)	5.1 (0.06)	
N4 (Expert)				**99.2 (3.7)**		3.7 (0.06)
R (Expert)	3.2 (0.03)	3.1 (0.05)	0.07 (0.02)		**94.6 (4.1)**	0.8 (0.02)
W (Expert)	3.5 (0.04)		0.06 (0.02)			**95.9 (4.7)**

All of our measures (F1 score, accuracy, sensitivity, and specificity) that evaluated the robustness of the proposed scheme for automatic sleep stage scoring based on a single sensor

were superior to previous attempts on the same dataset (Berthomier et al., 2007; Liang et al., 2012; Tsinalis et al., 2016). Complementarily, our methodology worked independently for N3 and N4 without merging them into a single stage.

Figure 7 illustrates the manually scored hypnogram of a subject versus the proposed single-sensor automatic sleep stage classification.

[**Figure 7 around here**]

3.3 Automatic Sleep Stage Classification Performance (ASSC) in an External Dataset

We also achieved very high classification accuracy, sensitivity and specificity for the second external dataset. Specifically, we achieved values of **95.1 ± 2.9%, 94.1 ± 3.1%,** and **94.0 ± 2.9%, respectively, across the subjects in the second dataset**. Complementarily, the mean F1 score was also high (91%, range 89–92%). The aforementioned results were followed by the application of the multi-class Naive Bayes classifier (with kernel) using as a training set the features extracted from the first dataset. All of our measures were averaged across subjects.

Table 3 demonstrates the averaged confusion matrix across the 77 subjects. Diagonal elements demonstrate the % of match between the expert and our algorithm, while off-diagonal elements illustrate the % of mismatch. The most correctly classified sleep stage was N4, followed by N3, W, N2, R and N1. Most misclassifications of N1 occurred in the R and W stages, for N2 in N3 and R, for N3 in R and W, for N4 in N3, for R in NI and N3 and for W in N4 and R.

Table 3. Averaged Confusion Matrix Across the 77 subjects based on the best-performing Fpz-Cz channel (%).

	N1 (Algorithm)	**N2 (Algorithm)**	**N3 (Algorithm)**	**N4 (Algorithm)**	**R (Algorithm)**	**W (Algorithm)**
N1 (Expert)	**94.5 (4.9)**				1.1 (0.05)	
N2 (Expert)		**94.2 (4.1)**				
N3 (Expert)	0.03 (0.04)	2.9 (0.05)	**97.6 (3.8)**	3.4 (0.04)	5.3 (0.07)	
N4 (Expert)				**96.8 (3.7)**		3.5 (0.07)

R (Expert)	3.0 (0.05)	3.2 (0.04)	2.1 (0.02)		**94.1 (4.1)**	1.7 (0.05)
W (Expert)	3.6 (0.04)		1.8 (0.02)			**95.1 (4.7)**

3.4 Relative Signal Power Changes during Sleep

Based on our results of relative signal power changes across the sleep stages (Fig. 7), low-δ {0.1-1.5 Hz} was elevated during deep sleep starting from N1 to N4. The signal power of high-δ (K-Complex) was higher in N1 and N2 and was decreased until REM. Complementarily, the signal power of θ {4-8 Hz} was higher in REM, which is an indicator of the activity of the brain during REM stage. We did not detect significant relative power changes in β_1 frequency across the sleep stages, especially in N2 linked to sleep spindles, possibly because of the long epoch of 5 sec.

3.5 Cross-Frequency Coupling Changes during Sleep

By combining Table 1 with Fig. 7, we revealed important tendencies of increased or decreased patterns of CFC with the four adopted estimators during the progression to deep sleep. For the PAC estimator, we detected higher values for the N3-N4 sleep stages, especially for slower brain rhythms (low-δ {0.1-1.5 Hz}, high-δ {1.6-4 Hz}, θ), while during REM, higher values were detected between θ-γ_1, α_1-α_2 and α_2-β_1. For the AAC estimator, the coupling for frequency pairs low-δ - high-δ, low-δ – θ and high-δ – θ was elevated during N3-N4, θ- α_1 was higher in N3 stage, α_1- α_2 and α_2- β_2 were higher in N4, and β_2- γ_1 was higher in REM. Complementarily, β_1- β_2 interactions were higher in N1, decreased in N2 and remained stable during N3-N4 and REM. The complex version of MI (CMI) worked better with the θ and α_2 brain rhythms, which further complemented the PAC estimates. Specifically, we observed higher values for low-δ- β_1 and high-δ- β_2 in the N3 stage, while θ- α_1 increased during deep sleep starting from N2 and continuing until N4. In contrast, θ- α_2 was higher in N2 and was decreased until N4. θ- β_1 demonstrated higher values for N3 and was further decreased in the N4 and REM stages. α_1- γ_1 demonstrated higher values in N1-N2 and then decreased until REM. α_2- β_1, α_2- β_2 and α_2- γ_1 increased during the first three sleep stages, reached a maximum in N3 and then further decreased until REM. Finally, the MI contributed to the multiparametric classifier with three features. Low-δ- high-δ demonstrated high values in the N1-N2-N3 sleep stages and was further reduced until the REM sleep. Low-δ- θ increased from N1 to N2 and

then reduced progressively until REM sleep. Finally, high-δ- θ was one of the detectable cross-frequency couplings in N1-N2 with MI with very low values in N3 and higher values in REM.

4 Discussion

In the present study, we demonstrated the feasibility of a novel single-sensor automatic sleep stage classification (ASSC) algorithm based on different aspects of cross-frequency coupling estimates. We achieved a very high classification sensitivity, specificity and accuracy of **90.3 ± 2.1%, 94.2 ± 2.3%,** and **94.4 ± 2.2% across 20 folds**, respectively, with a high mean F1 score (92%, range 90–94%) when a multi-class Naive Bayes classifier (with kernel) was applied. Our results revealed that the Fpz-Cz sensor is the most appropriate for ASSC, achieving better performance than Pz-Oz. Complementarily, we replicated our excellent results in an external second open-sleep database of 77 subjects. Specifically, we achieved very high classification accuracy, sensitivity and specificity of **95.1 ± 2.9%, 94.1 ± 3.1%,** and **94.0 ± 2.9%, respectively, across the subjects in the second dataset**. Additionally, the mean F1 score was high (91%, range 89–92%).

The entire methodology and the novelty of the proposed scheme can be summarized as follows:

- We analysed EEG recordings at every 5 s instead of 30 s epochs (which is the epoch length for the expert scoring).
- We kept N3 and N4 as single sleep stages without attempting to merge them (Tsinalis et al., 2016).
- We adopted MODWT to simultaneously decompose the EEG recordings into true activity assigned to one of the basic frequency ranges and to denoise the EEG recordings from eye movements and muscle activity.
- We adopted, apart from relative signal power, four different connectivity estimators (three phase-to-amplitude: PAC, MI, and CMI and one amplitude-to-amplitude: AAC).
- We used a dataset in which all the subjects (expect one) had more than one recording.
- A cross-validation scheme was designed for the following purposes:
    a) To access the generalizability of the method by adopting 20 folds in which at each fold, only the recordings from a single subject were used for training, while each subject's recordings were used only once for testing.
    b) To avoid imbalanced sleep stage distribution in the training set. For that purpose, we repeated the 20-fold CV 100 times by randomly sampling the class labels across sleep stages and subjects to keep their representation equal.

- Our results outperformed previous comparable studies on the same dataset (Berthomier et al., 2007; Liang et al., 2012; Tsinalis et al., 2016).
- We also replicated the proposed ASSC method based on CFC features in a second sleep dataset.
- We demonstrated, for the first time, the effectiveness of different cross-frequency coupling estimates for the improvement of CFC and a better understanding of the multiplexity of the human brain in sleep.

Our methodology presents a single-sensor automatic sleep stage classification based on cross-frequency coupling estimates that followed a very high classification performance. CFC outperformed trivial features derived from sleep recordings, further supporting the notion of CFC for sleep stage classification. A previous study attempted to demonstrate the positive effect of CFC on ASSC, achieving an overall accuracy of 75% with four sleep stages (Sanders et al., 2014). A more recent study explored phase-to-amplitude coupling in deep sleep and in epileptic patients, where elevated PAC was observed (Amiri et al., 2016).

Brain rhythms can interact with each other via different mechanisms, such as phase-to-phase, phase-to-amplitude (PAC) and amplitude-to-amplitude envelope correlation (see Figure 2 in Buszaki et al., 2012). Phase-to-phase coupling is an important mechanism that exists in a typical scenario in which two oscillators with the same or different frequency within the same or different anatomical brain area are entrained to each other. This mechanism can primarily be estimated between a pair of sensors and not within a single sensor (Dimitriadis et al., 2015b). A temporally less precise, but nevertheless important, brain interaction between oscillators of similar or different frequencies is expressed by the temporal covariation of their amplitude/power, known as amplitude/power comodulation or amplitude-amplitude/power-power coupling (correlation of the envelope: Bruns and Eckhorn, 2004).

The third basic mechanism for brain interactions is called frequency phase-to-amplitude (CPAC or PAC; Pittman-Polletta et al., 2014; Dimitriadis et al., 2015a, 2016 a, b) coupling of nested oscillations. One reason why slow oscillations couple faster brain rhythms in multiple brain areas is based on the conduction velocities of cortical neurons. Slower oscillators compared to more rapidly activate more neurons in a larger volume (von Stein and Sarnthein, 2000) and are associated with larger membrane potential changes since in longer temporal windows, a large portion of spikes of many more upstream neurons can be integrated (Hasenstaub et al., 2005; Quilichini et al., 2010). PAC has been reported between every pair of

brain rhythms in interactive circuits in the mammalian cortex from low oscillations, such as 0.025 Hz, up to fast ones, such as 500 Hz (Sirota et al., 2003).

The formation of new memories demands the coordination of neural activity across widespread brain regions. In both humans and animals, the hippocampus is believed to support the formation of new associative or contextually mediated memories (Clemens et al., 2009,Sirota and Buszaki,2005). During the consolidation of new memories at the system level, mnemonic representations of items initially rely on the hippocampus and after are thought to travel to neocortical sites for more permanent storage. Sleep has this privileged role for facilitating this information transfer (Born and Wilhelm, 2012). Mechanistically, consolidation processes have been demonstrated to rely on systematic interactions between the three basic neuronal oscillations that characterize non–rapid eye movement (NREM) sleep: slow oscillations, spindles and ripples (Staresina et al., 2015). Staresina et al. (2015) used direct intracranial EEG recordings from human epilepsy patients during natural sleep to test the assumption that slow oscillations, spindles and ripples are functionally coupled with hippocampal activity. They demonstrated a PAC between 0.5–1.25 Hz (slow oscillation range) and 12–16 Hz (spindle range) using the EEG modality and CZ sensor, respectively. In addition, they demonstrated a hippocampal PAC during NREM sleep stages, also providing a link between EEG-CZ recordings and hippocampal estimates from epileptic patients. The hierarchical role of these three sleep components (slow oscillations, spindles and ripples) was revealed via a PAC estimator.

A recent study untangled hippocampo-cortical CFC as the basic mechanism that mediates memory consolidation during sleep (Maingret et al., 2016). The authors provided a clear functional link between sharp-wave ripples, delta waves and ripples. Logothetis et al. (2012) demonstrated CFC-PAC coupling between hippocampo-cortical areas during a subcortical silence and off-line memory consolidation, while Amiri et al. (2016) demonstrated an enhanced PAC in deep sleep and in the onset zone of focal epilepsy.

Here, we selected the relative power of low-δ {0.1-1.5 Hz}, high-δ (K-Complex) {1.6-4 Hz} and θ {4-8 Hz} as complementary features to the CFC estimates for a better classification of the sleep stages (Table 3 and Fig. 6). δ waves were defined within the range of 1-4 Hz (Walker, 1990). Compared to the other brain waves, δ waves have the highest amplitude, while recent studies described slower (<0.1 Hz) oscillations (Hiltunen et al., 2014). Both sleep stages 3 and 4 are dominated by δ wave, with higher representation in sleep stage 4 (Iber et al., 2007). In addition, δ waves are often associated with another EEG phenomenon, the K-complex (high-δ: {1.6-4 Hz}). K-complexes have been demonstrated to precede δ waves in slow-wave sleep

(De Gennaro et al., 2000). Both K-complex and δ wave activity in sleep stage 2 generate both slow-wave (~0.8 Hz) and δ (1.6–4.0 Hz) oscillations. However, their topographical distribution is different, while the δ power of the K-complexes is higher (Happe et al., 2002). During sleep, θ activity appears as the prominent EEG activity in REM sleep, while θ activity serves as the background activity of both spindles and K-complexes during sleep stage 2 (Rodenbeck et al., 2006).

Our main goal was to further enhance the effort to achieve ASSC with high accuracy from a single sensor. It is also important to simultaneously study intra- and inter-frequency interactions, including phase-to-phase between multiple EEG sensors, to better understand the mechanisms and interactions that occur during sleep. It is important to mention here that our results were externally validated with a second large dataset, which makes the entire analysis stronger and unbiased from the subjective sleep scoring, based on which we trained our classifiers in the first dataset. Our next goal is to use an open database and to extend the present work and our previous work, in which we explored intra-frequency interactions between multiple EEG sensors during the five sleep stages (Dimitriadis et al., 2009).

Apart from the study of CFC interactions within a single sensor, the entire analysis was based on a healthy population. For that reason, our next goal is to explore brain connectivity during sleep stages using more EEG sensors and all the possible intra- and inter-frequency coupling modes. For that reason, we will work on the ISRUC database (multi-channels; Sirvan et al., 2016), which provides a large dataset from healthy individuals and sleep recordings from non-healthy individuals.

We demonstrated, for the first time, the effectiveness of different aspects of CFC, namely, PAC and amplitude-to-amplitude envelope correlation to automatically classify sleep stages (Tables 1 and Fig. 5). Additionally, we analysed sleep data under CFC in healthy populations for the first time, further demonstrating that CFC interactions exist during sleep and are altered during the transition between sleep stages. We achieved high classification accuracy in two datasets (training and testing datasets) using the activity recorded from a single EEG sensor. In the second study, we achieved lower mean classification accuracy across sleep stages compared to the first one, especially in the N4 and R sleep stages (Table 2 vs Table 3). One possible explanation for these findings could be the amplitude differences in slow oscillations between genders and across the lifespan (Mourtazaev et al., 1995). It is well known that ageing affects the neurophysiological generation of slow-wave oscillations (Leirer et al., 2011).

We also revealed multiple cross-frequency interactions between slow and medium frequencies and low γ activity in NREM sleep with every cross-frequency coupling estimator.

Our results further support that CFC during NREM sleep is a significant attribute of sleep and of overall memory consolidation.

To the best of our knowledge, our method achieved the best performance in the literature when classification was simultaneously performed across all five sleep stages and the wake (six class) condition using a single channel of EEG. This method is different from adopting a one-versus-all classification strategy, in which the classification performance is over-estimated. Our results also outperformed studies that used more than one channel (EOG, EEG, or EMG) to extract features for accurate sleep scoring. Our next goal is to test our algorithm on low-cost commercial EEG sensors (ear-EEG; Looney et al., 2016) and on recordings from home environments and to further explore CFC patterns in sleep disorders.

Conflict of Interest

The author(s) declare(s) that there is no conflict of interest regarding the publication of this paper.

Acknowledgements

SID and DL were supported by MRC grant MR/K004360/1 (Behavioural and Neurophysiological Effects of Schizophrenia Risk Genes: A Multi-locus, Pathway-Based Approach). SID is also supported by a MARIE-CURIE EU-UK COFUND FELLOWSHIP. Authors would like to thank the anonymous reviewers for their valuable comments that improve the quality of this study.

References

Aboalayon, K., Faezipour, M., Almuhammadi, W. and Moslehpour, S. (2016). Sleep Stage Classification Using EEG Signal Analysis:A Comprehensive Surveyand New Investigation. Entropy 18, p. 272.

Agarwal, R., and Gotman, J. (2001). Computer-assisted sleep staging. IEEE T.. Bio-med. Eng. 48, 1412-142.

Agarwal, R., and Gotman, J. (2002). Digital tools in polysomnography. J. Clin. Neurophysiol. 19, 136-143.

Allen, E.A., Liu, J.,Kiehl, K.A., Gelernter, J., Pearlson, G.D., Perrone-Bizzozero, N. I., et al. (2011). Components of cross-frequency modulation in health and disease. Front. Syst. Neurosci. 5:59. doi:10.3389/fnsys.2011.00059

Amiri M., Frauscher B., and Gotman, J. (2016). Phase-Amplitude Coupling Is Elevated in Deep Sleep and in the Onset Zone of Focal Epileptic Seizures. Front. Hum. Neuroscien 10. https://doi.org/10.3389/fnhum.2016.00387.

Antonakakis, M., Dimitriadis, S.I., Zervakis, M., Micheloyannis, S., Rezaie, R., Babajani-Feremi, A., Zouridakis, G., and Papanicolaou, A.C. (2016). Altered cross-frequency coupling in resting-state MEG after mild traumatic brain injury. Int. J. Psychophysiol. 102, 1-11. doi: 10.1016/j.ijpsycho.2016.02.002. Epub 2016 Feb 22

Axmacher, N., Henseler, M.M., Jensen, O., Weinreich, I., Elger, C.E., and Fell, J. (2010). Cross-frequency coupling supports multi-item working memory in the human hippocampus. P Natl Acad Sci USA 107, 3228–3233. doi: 10.1073/pnas.0911531107

Becq, G., Charbonnier, S., Chapotot, F., Buguet, A., Bourdon, L., and Baconnier, P. (2005). Comparison between five classifiers for automatic scoring of human sleep recordings. SCI 4, 113-127

Berthomier, C., Drouot, X., Herman-Stoïca, M., Berthomier, P., Prado, J., Bokar-Thire, et al. (2007). Auto-matic analysis of single-channel sleep EEG: validation in healthy individuals. Sleep 30, 1587-1595.

Born J., and Wilhelm I. (2012). System consolidation of memory during sleep. Psychol. Res. 76, 192-203. doi:10.1007/s00426-011-0335-6.

Brignol, A., Al-Ani, T., and Drouot X. (2012). EEG-based automatic sleep-wake classification in humans using short and standard epoch lengths. In Proceedings of the 12th IEEE International Conference on Bioinformatics & Bioengineering (BIBE), 276–281, Larnaca, Cyprus.

Bruns, A., and Eckhorn, R. (2004). Task-related coupling from high to low-frequency signals among visual cortical areas in human subdural recordings. Int. J. Psychophysiol. 51, 97–116. doi: 10.1016/j.ijpsycho. 2003. 07.001

Buzsáki, G. (2010). Neural syntax: cell assemblies, synapsembles, and readers, Neuron 68, 362–385. doi: 10.1016/j.neuron.2010.09.023

Buzsáki, G., Logothetis, N., and Singer, W. (2013). Scaling brain size, keeping timing: evolutionary preservation of brain rhythms. Neuron 80, 751–764. doi: 10.1016/j.neuron.2013.10.002

Bruns, A., Eckhorn, R., Gail, A., Brinksmeyer, H.J., and Schanze, T., (2001). Directional coupling of gamma-envelopes and theta-signals between separate neuronal populations in human and monkey visual cortex. Soc. Neurosci. Abstr. 27, 36

Buzsaki, G., and Draguhn, A. (2004). Neuronal oscillations in cortical networks. Science 304, 1926–1929. doi:10.1126/science.1099745

Buzsáki G, and Watson, BO. (2012). Brain rhythms and neural syntax: implications for efficient coding of cognitive content and neuropsychiatric disease. Dialogues Clin. Neurosci. 14, 345-367.

Canolty, R.T., Edwards, E., Dalal, S.S., Soltani, M., Nagarajan, S.S., Kirsch, H.E., et al. (2006). High gamma power is phase-locked to theta oscillations in human neo cortex. Science 313, 1626–1628. doi:10.1126/science.1128115

Canolty, R.T., and Knight, R.T. (2010). The functional role of cross-frequency coupling. Trends Cogn. Sci. 14, 506-515.

Cash S.S.; Halgren E.; Dehghani N., , Rossetti A.O., Thesen, T., Wang, C., et al. (2009). "Human K-Complex Represents an Isolated Cortical Down-State". Science. 324 (5930): 1084–87.

Chang, C.C., and Lin, C.J. (2011). LIBSVM : a library for support vector machines. ACM T. Intel. Syst. Tec. 2, 27.

Dang-Vu TT, McKinney SM, Buxton OM, Solet JM, JM Ellenbogen**Spontaneous brain rhythms predict sleep stability in the face of noise**.Curr Biol, 20 (2010), pp. R626-R627

De Gennaro, L., Ferrara, M., and Bertini, M. (2000). The spontaneous K-complex during stage 2 sleep: is it the 'forerunner' of delta waves ?. Neurosci. Lett. 291, 41–43.

Deng, C., Chiyuan, Z., and Xiaofei, He. (2010). Unsupervised Feature Selection for Multi-cluster Data. 16th ACM SIGKDD Conference on Knowledge Discovery and Data Mining (KDD'10), Washington DC, DC, USA.

Clemens Z.,Weiss B., Szucs A., Eross L., Rásonyi G, and Halász P. (2009). Phase coupling between rhythmic slow activity and gamma characterizes mesiotemporal rapid-eye-movement sleep in humans. J. Neurosci. 163, 388–396.

Dursun, M., Gunes, S., Ozsen, S., and Yosunkaya, S. (2012). Comparison of artificial immune clustering with fuzzy c-means clustering in the sleep stage classification problem. In Proceedings of the International Symposium on Innovations in Intelligent Systems and Applications (INISTA), 1–4, Trabzon, Turkey.

Dimitriadis, S.I., Laskaris, N.A., Del Rio-Portilla, Y., and Koudouni G.C. (2009) Characterizing dynamic functional connectivity across sleep stages from EEG. Brain Topogr. 22, 119–133.

Dimitriadis, S.I., Laskaris, N.A., Bitzidou, M.P., Tarnanas, I., and Tsolaki, M.N (2015a). A novel biomarker of amnestic MCI based on dynamic cross-frequency coupling patterns during cognitive brain responses. Front. Neurosci-Switz 9:350. doi: 10.3389/fnins.2015.00350

Dimitriadis, S. I., Sun, Y. U., Kwok, K., Laskaris, N. A., Thakor, N., and Bezerianos, A. (2015a). Cognitive workload assessment based on the tensorial treatment of EEG estimates of cross-frequency phase interactions. Ann. Biomed. Eng. 43, 977–989. doi: 10.1007/s10439-014-1143-0

Dimitriadis, SI, Laskaris, N.A., Simos, P.G., Fletcher, J.M., and Papanicolaou, A.C. (2016a). Greater Repertoire and Temporal Variability of Cross-Frequency Coupling (CFC) Modes in Resting-State Neuromagnetic Recordings among Children with Reading Difficulties, Front. Hum. Neurosci. 10, 163. doi: 10.3389/fnhum.2016.00163

Dimitriadis, S.I., Tarnanas, I., Wiederhold, M., Wiederhold, B., Tsolaki, M, and Fleisch, E. (2016b). Mnemonic strategy training of the elderly at risk for dementia enhances integration of information processing via cross-frequency coupling. Alzheimer's Dement: TRCI 2, 241–249

Ebrahimi, F., Mikaeili, M., Estrada, E., Nazeran, H. (2008). Automatic sleep stage classification based on EEG signals by using neural networks and wavelet packet coefficients. In Proceedings of the 30th IEEE EMBS Annual International Conference of the Engineering in Medicine and Biology Society, 1151–1154, Vancouver, BC, Canada.

Estrada, E., Nazeran, H., Nava, P., Behbehani, K., Burk, J., and Lucas, E. (2004). EEG feature extraction for classification of sleep stages. In Proceedings of the 26th IEEE EMBS Annual International Conference of the engineering in Medicine and Biology Society, 196–199, San Francisco, CA, USA.

Fell, J., Röschke, J., Mann, K., and Schäffner, C. (1996). Discrimination of sleep stages: A comparison between spectral and nonlinear EEG measures. Electroen. Clin. Neuro. 98, 401–410.

Fries, P. (2005). A mechanism for cognitive dynamics: neuronal communication through neuronal coherence. Trends Cogn. Sci. 9, 474–480.doi: 10.1016/j.tics.2005.08.011

Goldberger, A. L., Amaral, L. A. N., Glass, L., Hausdorff, J. M., Ivanov, P. C., Mark, et. al. (2000). PhysioBank, PhysioToolkit, and PhysioNet: Components of a new research resource for complex physiologic signals. Circulation 101, 215–220.

Gudmundsson, S., Runarsson, T.P., and Sigurdsson, S. (2005). Automatic sleep staging using support vector machines with posterior probability estimates. InConcur. Syst, Engn. Ser. , 2005 and International Conference on Intelligent Agents, Web Technologies and Internet Commerce, International Conference on, 366–372, Washington, DC, USA.

Güneş, S., Polat, K., and Yosunkay S. (2010). Efficient sleep stage recognition system based on EEG signal using k-means clustering based feature weighting. Expert Syst. Appl. 37, 7922-7928.

Happe, S., Anderer, P., Gruber, G.; Klösch, G., Saletu, B. and Zeitlhofer, J. (2002). Scalp topography of the spontaneous K-complex and of delta-waves in human sleep. Brain Topogr. 15:1, 43–9. doi:10.1023/A:101999252324

Hasenstaub, A., Shu, Y., Haider, B., Kraushaar, U., Duque, A., and McCormick, DA. (2005). Inhibitory postsynaptic potentials carry synchronized frequency information in active cortical networks. Neuron 47, 423–435.

Hiltunen, T., Kantola, J., Abou, Elseoud A., Lepola, P., Suominen, K., Starck, T. et al. (2014). Infra-slow EEG fluctuations are correlated with resting-state network dynamics in fMRI. J. Neurosci. 34, 356-362.

Hobson, J.A. (1969). A manual of standardized terminology, techniques and scoring system for sleep stages of human subject. Electroen. Clin. Neuro. 26, 644.

Huang, C., Davis, L.S., and Townshend, J.R.G. (2002). An assessment of support vector machines for land cover classification. Int. J. Remote Sens. 23, 725-749.

Huang, C.S., Lin, C.L., Ko, L.W., Liu, S.Y., Sua, T.P., Lin, C.T. (2013). A hierarchical classification system for sleep stage scoring via forehead EEG signals. In Proceedings of the IEEE Symposium on Computational Intelligence, Cognitive Algorithms, Mind, and Brain (CCMB), 1–5, Singapore.

Huang, G.B., Zhou, H., Ding, X., and Zhang, R. (2010). Extreme Learning Machine for Regression and Multiclass Classification. IEEE T. Syst. Man Cy. B 42, 513-529.

Jensen, O., and Colgin, L.L. (2007). Cross-frequency coupling between neuronal oscillations. Trends Cogn. Sci. 11, 267–269. doi:10.1016/j.tics.2007.05.003.

pey

Iber, C, Ancoli-Israel, S, Chesson, AL, and Quan, SF. The AASM manual for the scoring of sleep and associated events: rules, terminology, and technical specification. AASM, Westchester, Illinois, USA, 2007.

Itil, T., Shapiro, D., Fink, M. and Kassebaum, D. (1969). Digital computer classifications of EEG sleep stages. Electroen. Clin. Neuro. 27, no. 1, pp. 76-83.

Kemp, B., Zwinderman, A. H., Tuk, B., Kamphuisen, H. A. C., Oberye, J. J. L. (2000). Analysis of a sleep-dependent neuronal feedback loop: The slow-wave microcontinuity of the EEG. IEEE T. Bio-med. Eng. 47, 1185–1194.

Khalighi, S., Sousa, T., Oliveira, D., Pires, G., and Nunes, U. (2011). Efficient feature selection for sleep staging based on maximal overlap discrete wavelet transform and SVM. In Proceedings of the 33rd IEEE EMBS Annual International Conference of the Engineering in Medicine and Biology Society, 3306–3309, Boston, MA, USA.

Koley, B., and Dey, D. (2012). An ensemble system for automatic sleep stage classification using single channel EEG signal. Comput Biol Med 42, 1186-1195.

Krakovská, A., and Mezeiová, K. (2011). Automatic sleep scoring: A search for an optimal combination of measures. Artif Intell Med 53, 25-33.

Kuo, C.E., and Liang, S.F. Automatic stage scoring of single-channel sleep EEG based on multiscale permutation entropy. In Proceedings of the IEEE Conference on Biomedical Circuits and Systems (BioCAS), 448–451, San Diego, CA, USA.

Lajnef, T., Chaibi, S. , Ruby, P. , Aguera, P.E., Eichenlaub, J.B. , Samet, et al. (2015). Learning machines and sleeping brains: Automatic sleep stage classification using decision-tree multi-class support vector machines. J. Neurosci. Methods 250, 94-105.

Lachaux, J. P., Rodriguez, E., Martinerie, J., and Varela, F. J. (1999). Measuring phase synchrony in brain signals. Hum Brain Mapp 8, 194–208.

Lan, K.C., Chang, D.W., Kuo, C.E., Wei, M.Z., Li, Y.H., Shaw, F.Z. et al. (2015). Using off-the-shelf lossy compression for wireless home sleep staging. J. Neurosci. Methods 246, 142–152.

Lainscsek, C., Val´erie M., Portman, A., Muir, J.F., Sejnowski, T.J., and Letellier, C. (2013). Automatic sleep scoring from a single electrode using delay differential equations. In 12TH CONFERENCE on Dynamical Systems Theory and Applications (DSTA), L´od´z, Poland.

Larsen, L. and Walter, D. (1970). On automatic methods of sleep staging by EEG spectra. Electroen. Clin. Neuro. 28, 459-467.

Leirer, V.M., Wienbruch, C., Kolassa, S, Schlee, W., Elbert, T., Kolassa, I.T. (2011). Changes in cortical slow wave activity in healthy aging. Brain Imaging Behav. 5, 222-228. doi: 10.1007/s11682-011-9126-3.

Li, Y., Yingle, F., Gu, L., and Qinye, T. (2009). Sleep stage classification based on EEG Hilbert–Huang transform. In Proceedings of the 4th IEEE Conference on Industrial Electronics and Applications (ICIEA), 3676–3681, Xi'an, China.

Liang, S.F., Kuo, C.E., Hu, Y.H., Pan, Y.H., Wang, Y.H. (2012). Automatic stage scoring of single-channel sleep EEG by using multiscale entropy and autoregressive models. IEEE T. Instrum. Meas. 61, 1649–1657.

Liu, Y., Yan, L., Zeng, B., and Wang, W. (2010). Automatic sleep stage scoring using Hilbert–Huang transform with BP neural network. In Proceedings of the 4th International Conference on Bioinformatics and Biomedical Engineering (iCBBE), 1-4, Chengdu, China.

Logothetis, N. K., Eschenko, O., Murayama, Y., Augath, M., Steudel, T., Evrard, H.C. et al. (2012). Hippocampal–cortical interaction during periods of subcortical silence. Nature 491,547–553. doi:10.1038/nature11618

Looney, D., Goverdovsky, V., Rosenzweig, I., Morrell, M. J., and Mandic, D. P. (2016). A Wearable In-Ear Encephalography Sensor for Monitoring Sleep: Preliminary Observations from Nap Studies. Ann. Am. Thorac. Soc. 13, 2229-2233.

Ma, Haoyu, Hu, Bin, Jackson, Mike, Yan, Jingzhi, and Zhao, Wen. (2011). A hybrid classification method using artifi-cial neural network based decision tree for automatic sleep scoring. World Acad. Sci. Eng. Technol. 79, 279-284.

Maingret N, Girardeau G, Todorova R, Goutierre M, Zugaro M.(2016).**Hippocampo-cortical coupling mediates memory consolidation during sleep.** Nat. Neurosci., 19 , 959-964

Mourtazaev, MS, Kemp, B, Zwinderman, AH, Kamphuisen, HA. (1995). Age and gender affect different characteristics of slow waves in the sleep EEG. Sleep 18, 557-64.

Formatted: French (France)
Formatted: French (France)
Formatted: German (Germany)
Formatted: German (Germany)
Field Code Changed
Field Code Changed
Formatted: German (Germany)
Formatted: German (Germany)
Formatted: German (Germany)
Field Code Changed
Formatted: German (Germany)
Formatted: German (Germany)
Field Code Changed
Formatted: German (Germany)
Formatted: German (Germany)
Formatted: German (Germany)
Field Code Changed
Formatted: German (Germany)
Formatted: German (Germany)
Field Code Changed

Nolte, G., Bai, O., Wheaton, L., Mari, Z., Vorbach, S., and Hallet, M. (2009). Identifying true brain interaction from EEG data using the imaginary part of coherency. J. Clin. Neurophysiol. 115, 2292–2307. doi: 10.1016/j.clinph.2004.04.029

Pan, S.T., Kuo, C.E., Zeng, J.H., Liang, S.F. (2012). A transition-constrained discrete hidden Markov model for automatic sleep staging. Biomed. Eng. Online 11, 11-52.

Panossian, LA, and Avidan, AY. (2009). Review of sleep disorders. Med. Clin. N. Am. 93, 407-425.

Peyrache, A. (2011). Inhibition recruitment in prefrontal cortex during sleep spindles and gating of hippocampal inputs. P. Natl. Acad. Sci. USA. 108, 17207.

Phan, H., Do, Q., Do, T.L., and Vu, D.L. (2013). Metric learning for automatic sleep stage classification. In Proceedings of the 35th IEEE Annual International Conference of the Engineering in Medicine and Biology Society (EMBC), 5025–5028, Osaka, Japan.

Pittman-Polletta, B., Hsieh, W.H., Kaur, S., MT, Lo, and Hu, K. (2014). Detecting phase-amplitude coupling with high frequency resolution using adaptive decompositions. J. Neurosci. Meth. 226, 15–32.doi: 10.1016/j.jneumeth.2014.01.006

Quilichini P., Sirota A., Buzsaki G. (2010). Intrinsic circuit organization and theta-gamma oscillation dynamics in the entorhinal cortex of the rat. J Neurosci. 30, 11128–11142.

Rodenbeck, A., Binder, R., Geisler, P., Danker-Hopfe, H., Lund, R., Raschke, F. (2006). A review of sleep EEG patterns. Part I: A compilation of amended rules for their visual recognition according to Rechtschaffen and Kales. Somnologie 10, 159-175.

Schaltenbrand, N., Lengelle, R., Toussaint, M., Luthringer, R., Carelli, G., Jacqmin, A. et al. (1996). Sleep stage scoring using the neural network model: comparison between visual and automatic analysis in normal subjects and patients. Sleep 19, 26-35.

Sheng-Fu, L., Chin-En, K., Yu-Han, H., and Yu-Shian, C. (2012). A rule-based automatic sleep staging method. J. Neurosci. Meth. 205, 169-176.

Sirota, A., Csicsvari, J., Buhl, D., Buzsaki, G. (2003). Communication between neocortex and hippocampus during sleep in rodents. P. Natl. Acad. Sci. USA 100, 2065–2069.

Sirota, A., and Buzsaki, G. (2005). Interaction between neocortical and hippocampal networks via slow oscillations. Thalamus Relat. Sys. 3, 245–259.

Sirvan, K., Sousa, T., Santos, J.M., and Nunes, Urbano. (2016). ISRUC-Sleep: A comprehensive public dataset for sleep researchers. Comput Meth. Progr. Bio. 124, 180-192.

Saletin, J.M.; Goldstein, A.N.; Walker, M.P (2011). The Role of Sleep in Directed Forgetting and Remembering of Human memories. Cereb. Cortex, 21, 2534–2541

Sanders, T.H., McCurry, M., Clements, and Mark A. (2014). Sleep stage classification with cross frequency coupling. Engineering in Medicine and Biology Society (EMBC), 2014 36th Annual International Conference of the IEEE, Chicago, IL, USA.

Sen, B., Peker, M., Çavuşoğlu, A., and Çelebi, F.V. (2014). A comparative study on classification of sleep stage based on EEG signals using feature selection and classification algorithms. J. Med. Syst. 38, 1–21.

Sousa, T., Cruz, A., Khalighi, S., Pires, G., and Nunes, U. (2015). A two-step automatic sleep stage classification method with dubious range detection. Comput. Biol. Med. 59, 42–53.

Stanus, E., Lacroix, B., Kerkhofs, M., and Mendlewicz, J. (1987). Automated sleep scoring: a comparative reliability study of two algorithms. Electroen.. Clin. Neuro. 66, 448-456.

Staresina, B.P., Bergmann, T.O., Bonnefond, M., van der Meij, R., Jensen Ole, Deuker, L., et al. Hierarchical nesting of slow oscillations, spindles and ripples in the human hippocampus during sleep. Nat. Neurosci. 18, 1679–1686 (2015).

Steriade, Mircea, and McCarley, R.W., (1990). Brainstem Control of Wakefulness and Sleep, New York: Plenum Press.

Steriade, M., Nunez, A. & Amzica, F. A novel slow (< 1 Hz) oscillation of neocortical neurons *in vivo*: depolarizing and hyperpolarizing components. *J. Neurosci.* **13**, 3252–3265 (1993)

Šušmáková, K., and Krakovská, A. (2008). Discrimination ability of individual measures used in sleep stages classification. Artif Intell Med. 44, 261-277.

"The Sleep-EDF Database [Expanded]", Physionet.org, 2017. [Online]. Available: http://www.physionet.org/physiobank/database/sleep-edfx/. Accessed Jan 2015.

Tamminen, J.; Payne, J.D.; Stickgold, R.; Wamsley, E.J.; Gareth Gaskell, M. (2010). Sleep spindle activity is associated with the integration of new memories and existing knowledge. J. Neurosci., 30(43), 14356–60

Tort, A.B., Kramer, M.A., Thorn, C., Gibson, D.J., Kubota, Y., Graybiel, A. M., et al. (2008). Dynamic cross-frequency couplings of local field potential oscillations in rat striatum and hippocampus during performance of a T-maze task. P. Natl. Acad. Sci .U.S.A. 105, 20517–20522.doi: 10.1073/pnas.0810524105

Tort, A.B.L., Komorowski, R., Eichenbaum, H., and Kopell, N. (2010). Measuring Phase-Amplitude Coupling Between Neuronal Oscillations of Different Frequencies. J Neurophysiol. 104, 1195-1210. doi:10.1152/jn.00106.2010.

Tsai, P.Y., Hu, W., Kuo, T.B., and Shyu, L.Y. (2009). A portable device for real time drowsiness detection using novel active dry electrode system. In Proceedings of the 31st IEEE EMBS Annual International Conference of the Engineering in Medicine and Biology Society, 3775–3778, Minneapolis, MN, USA.

Tsinalis, O, Matthews, P.M., and Guo, Y. (2016). Automatic Sleep Stage Scoring Using Time-Frequency Analysis and Stacked Sparse Autoencoders. Ann. Biomed. Eng. 44, 1587–1597.

Von Stein, A., and Sarnthein, J. (2000). Different frequencies for different scales of cortical integration: from local gamma to long range alpha/theta synchronization. Int. J. Psychophysiol. 38, 301–313. doi:10.1016/S0167- 8760(00)00172-0

Voytek, B., Canolty, R.T., Shestyuk, A., Crone, N.E., Parvizi, J., and Knight, R.T. (2010). Shifts in Gamma Phase–Amplitude Coupling Frequency from Theta to Alpha Over Posterior Cortex During Visual Tasks. Front. Hum. Neurosci. 4, 191.

Walker, P. (1999). Chambers dictionary of science and technology. Edinburgh: Chambers, 312.

Weiss, B., Clemens, Z., Bódizs, R., and Halász, P. (2011). Comparison of fractal and power spectral EEG features: Effects of topography and sleep stages. Brain Res. Bull. 84, 359–375.

Yu, S., Chen, X., Wang, B., and Wang, X. (2012). Automatic sleep stage classification based on ECG and EEG features for day time short nap evaluation. In Proceedings of the 10th World Congress on Intelligent Control and Automation (WCICA), 4974–4977, Beijing, China.

Zhovna, I., and Shallom, I.D. (2008). Automatic detection and classification of sleep stages by multichannel EEG signal modelling. In Proceedings of the 30th IEEE EMBS 2008 Annual International Conference of the IEEE Engineering in Medicine and Biology Society, 2665–2668, Vancouver, BC, Canada.

Zoubek, L., Charbonnier, S., Lesecq, S., Buguet, A., and Chapotot, F. (2007). Feature selection for sleep/wake stages classification using data driven methods. Biomed Signal Process Control 2, 171–179

Figure Captions

Figure 1. Outline of the methodology.

Figure 2. Algorithmic steps for PAC estimation. Using the first-epoch EEG signal from the Fpz-Cz sensor of subject 1 during the wake condition **(A)**, we demonstrated the phase-to-amplitude coupling between θ and β_1 rhythms. First, the raw time series was bandpass filtered using a zero-phase-order filter into **(B)** a low-frequency θ (4–8 Hz) component, where its envelope (Hilbert transform) was extracted and into **(C)** a high-frequency β_1 (13–20 Hz) component, where its phase dynamics were estimated via Hilbert transform. **(D)** We then estimated both the amplitude and the instantaneous phase of the bandpassed β_1 (13–20 Hz) component, and we filtered the amplitude of this time series within the θ frequency range (4–8 Hz). This algorithmic step will provide us with the θ modulation within the lower β amplitude. **(E)** Subsequently, we Hilbert transformed both the θ-filtered signal and the θ-filtered within the lower-β amplitude, extracting the related phase dynamics and, finally, their phase consistency with iPLV. The phase differences of those two phase time series, which are illustrated in **(F)**, will be the input in the iPLV estimator to quantify the strength of PAC coupling between θ and β_1 rhythms and to determine how the phase of the lower-frequency component modulates the amplitude of the high-amplitude component.

Figure 3. Algorithmic steps for AAC estimation. Using the first-epoch EEG signal from the Fpz-Cz sensor of subject 1 during the wake condition **(A)**, we demonstrated the detection of coupling between θ and β_1 rhythms. To estimate θ-β_1 AAC, the raw signal was bandpass filtered into both **(B)** a high-frequency β_1 (13–20 Hz) component, where its envelope was extracted, and **(C)** a low-frequency θ (4–8 Hz) component, where its envelope was also extracted. **(D)** We then presented the envelopes of the bandpassed θ (4–8 Hz) and β_1 (13–20 Hz) into a common plot. **(E)** Finally, we estimated the point-wise squared time series of the envelopes to obtain the power time series. The AAC was estimated on these power time series using correlation coefficient.

Figure 4. Algorithmic steps for CMI estimation. Using the first-epoch EEG signal from the Fpz-Cz sensor of subject 1 during the wake condition **(A)**, we demonstrated the detection of coupling between θ and β_1 rhythms. To estimate θ-β_1 CMI, the raw signal was bandpass filtered into **(B)** a low-frequency θ (4–8 Hz) component, where its phase was extracted, and into **(C)** a high-frequency β_1 (13–20 Hz) component, where its amplitude was presented. **(D)** The mean amplitude of the high-frequency component was estimated within each **(E)** phase bin extracted from the phase of the low-frequency component. The CMI was estimated based on the average complex values of mean amplitude and mean phase within each bin. Here, we used 20 phase bins.

Fig. 5. Illustration of the comodulograms of the four CFC estimators adopted in the present study averaged across epochs at each sleep stage and wake condition from a single subject. On the x-axis are the frequencies of the modulator, while on the y-axis are the frequencies of the modulated brain rhythm. (NREM1-4: N1, N2, N3, and N4; R: REM; W: WAKE; Frequencies 1-8: 1: low-δ {0.1-1.5 Hz}, 2: high-δ (K-Complex) {1.6-4 Hz}, 3: θ {4-

8 Hz}, 4: α_1 {8-10 Hz}, 5: α_2 {10-13 Hz}, 6: β_1 (spindle) {14-20 Hz}, 7: β_2 {21-30 Hz} and 8: γ_1 {31 – 45 Hz}). Averaged comodulograms across sleep stages and the wake condition are illustrated in (A) PAC, (B) AAC, (C) CMI and (D) MI **(E)** A graphical layout of a comodulogram for a better understanding the notion of CFC estimates. Nodes represent the modulating brain rhythms, the arrows are directed to the modulated frequencies, and the colour indicates the strength of PAC. At each epoch of 5 sec and for each of the four cross-frequency coupling estimates, all possible pair-wise frequency interactions were estimated, as shown in the graphical representation. PAC couplings have been estimated for the first epoch of the N1 sleep stage of subject 1 in the first dataset.

Fig. 6. **Illustration of the relative power (RP) averaged across epochs at each sleep stage and wake condition from a single subject**. On the x-axis, the RP of eight frequency bands are presented in six blocks. (NREM1-4: N1, N2, N3, and N4; R: REM; W: WAKE; Frequencies 1-8: 1: low-δ {0.1-1.5 Hz}, 2: high-δ (K-Complex) {1.6-4 Hz}, 3: θ {4-8 Hz}, 4: α_1 {8-10 Hz}, 5: α_2 {10-13 Hz}, 6: β_1 (spindle) {14-20 Hz}, 7: β_2 {21-30 Hz} and 8: γ_1 {31 – 45 Hz}). We denoted with '*' the significant differences of RP across the frequencies at every sleep stage and wake condition. Frequencies α_1 , α_2 , β_1 ,β_2 and γ_1 were grouped to enhance the visualization of significant trends (* Wilcoxon Rank Sum Test, $p < 0.01$, Bonferroni corrected $p' < p/28$ where 28 denotes the possible pairs of the 8 frequencies)

Fig. 7. Manual scoring versus automatic sleep stage scoring.
On the top, we illustrate the original manually scored hypnogram, while on the bottom, we illustrate the estimated hypnogram using the proposed algorithm for the second night of subject 1.

Figure 1

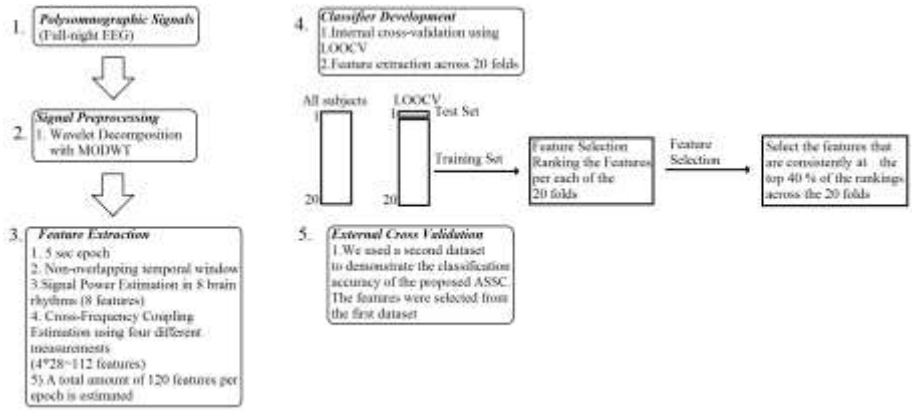

Figure 2

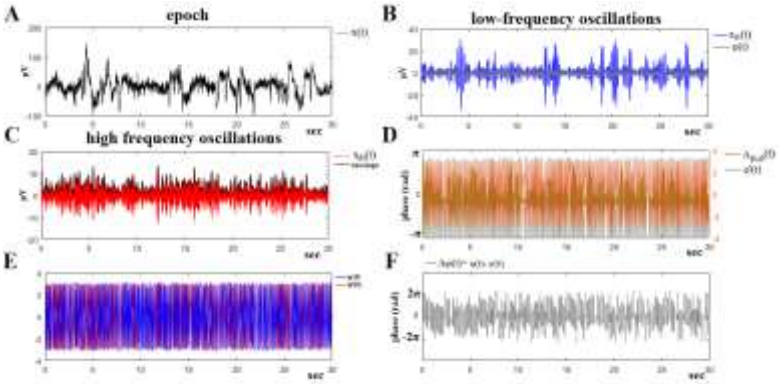

Figure 3

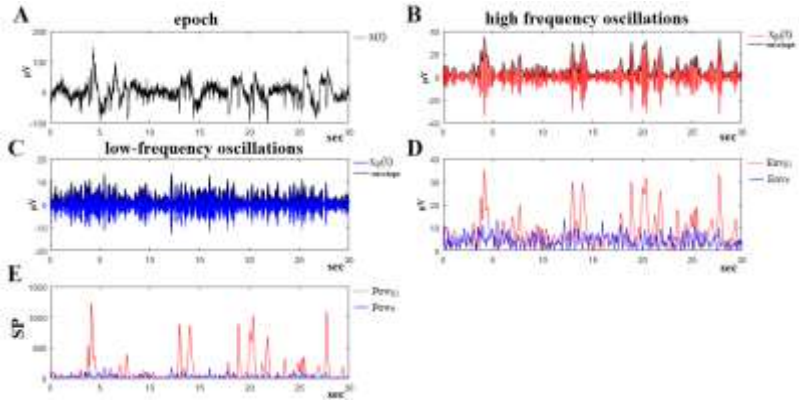

Figure 4

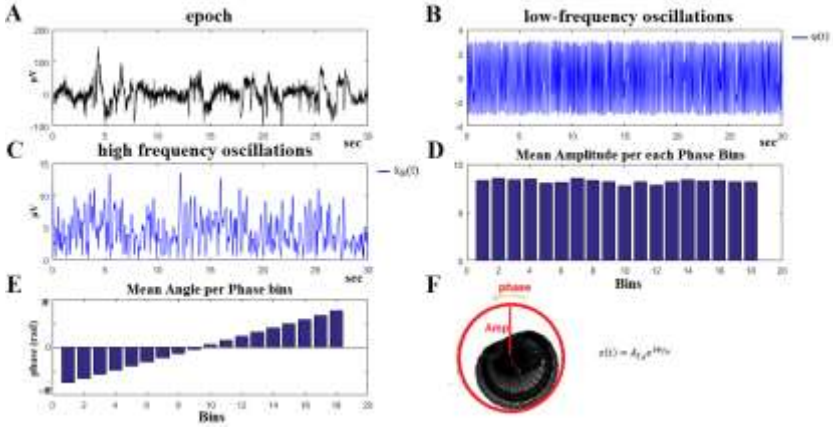

Figure 5

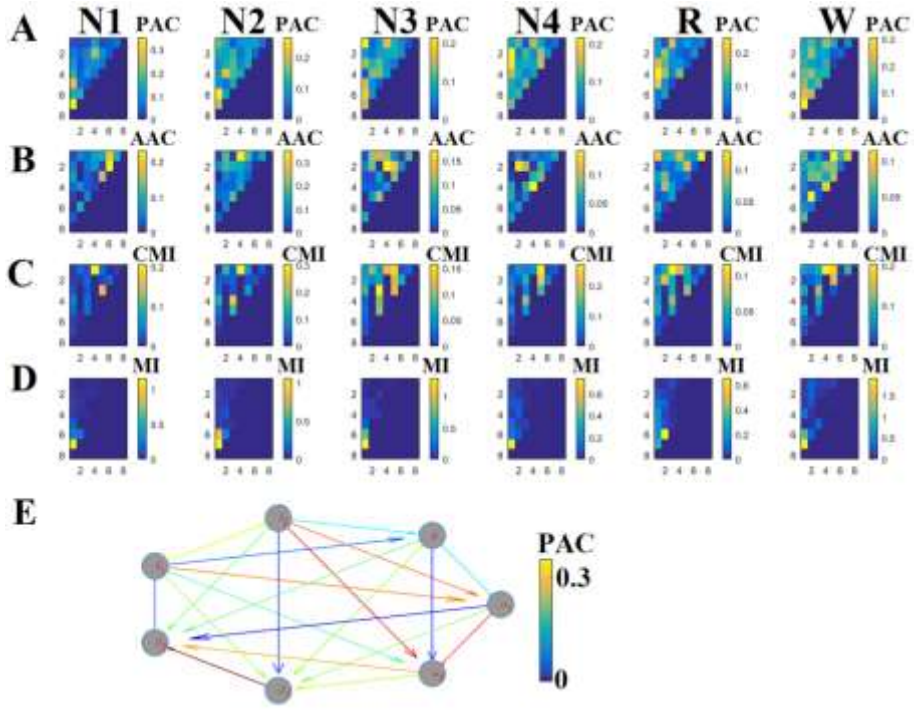

Figure 6

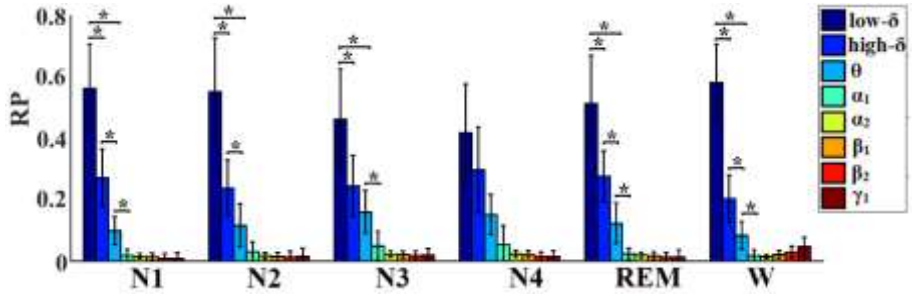
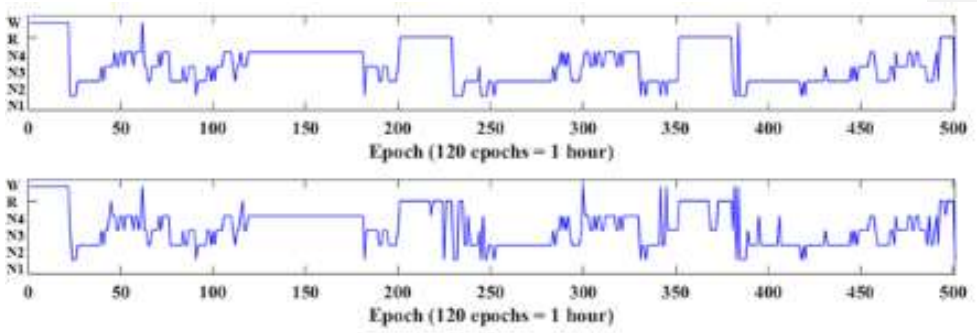
Figure 7